Cryptophyte farming by symbiotic ciliate host detected in situ

Dajun Qiu[a], Liangmin Huang[a], and Senjie Lin[b,1]

[a]Chinese Academy of Sciences Key Laboratory of Tropical Marine Bio-Resources and Ecology, South China Sea Institute of Oceanology, Chinese Academy of Sciences, Guangzhou 510301, China; and [b]Department of Marine Sciences, University of Connecticut, Groton, CT 06340

Edited by David M. Karl, University of Hawaii, Honolulu, HI, and approved September 8, 2016 (received for review July 28, 2016)

Protist–alga symbiosis is widespread in the ocean, but its characteristics and function in situ remain largely unexplored. Here we report the symbiosis of the ciliate *Mesodinium rubrum* with cryptophyte cells during a red-tide bloom in Long Island Sound. In contrast to the current notion that *Mesodinium* retains cryptophyte chloroplasts or organelles, our multiapproach analyses reveal that in this bloom the endosymbiotic *Teleaulax amphioxeia* cells were intact and expressing genes of membrane transporters, nucleus-to-cytoplasm RNA transporters, and all major metabolic pathways. Among the most highly expressed were ammonium transporters in both organisms, indicating cooperative acquisition of ammonium as a major N nutrient, and genes for photosynthesis and cell division in the cryptophyte, showing active population proliferation of the endosymbiont. We posit this as a "*Mesodinium*-farming-*Teleaulax*" relationship, a model of protist–alga symbiosis worth further investigation by metatranscriptomic technology.

cryptophyte *Teleaulax* | *Mesodinium rubrum* | red-tide bloom | intact endosymbiont | metatranscriptome

Protist–alga symbiosis is much more widespread in the marine ecosystem than previously thought, both spatially and taxonomically (1). Such biotic relationships are ecologically important, because they either fix nitrogen to provide N nutrients to sustain host photosynthesis (in the case of eukaryotic plankton harboring diazotrophic cyanobacteria) or photosynthesize to provide the host with organic carbon (in the case of heterotrophic protist-harboring algae). Field and laboratory observations have documented a wide range of host integration of symbionts, from enslaving transiently kept chloroplasts (so-called kleptoplastids) to permanent intact-cell endosymbionts (2). However, the degree of host integration and function of endosymbionts in natural plankton assemblages in situ is poorly understood and severely understudied, because such studies are very challenging. One example is the ciliate *Mesodinium rubrum*, a widely distributed marine protist, known to feed upon cryptophyte algae and retain their chloroplasts for photosynthesis (3–12). *M. rubrum* can form massive blooms of up to 10^6 cells L^{-1} in coastal and estuarine waters, and the retained plastid contributes up to 70% of primary productivity under some conditions (5–7). Based on field observations and laboratory studies, a wide range of relationships between this ciliate and its cryptophyte symbiont has been reported, including retention of not only the cryptophyte chloroplast but also the nucleus (8–10), endoplasmic reticulum (10, 11), and plastid–mitochondrion complexes (9–12). Whole cryptophyte cells in the ciliate host have also been observed (2, 13, 14), although it is unclear whether they represent predigested prey algae. Applying environmental transcriptomics and other methods to a natural bloom of *M. rubrum*, we found that the ciliate population in this bloom hosted intact and actively reproducing cells of *Teleaulax amphioxeia* expressing genes of membrane transporters, nucleus-to-cytoplasm RNA transporters, and all major metabolic pathways, indicating an unsuspected relationship of "*Mesodinium* farming *Teleaulax*."

Results and Discussion

A red-tide bloom occurred in Long Island Sound in September of 2012 (Fig. 1*A*). Microscopic examination revealed *M. rubrum* as the causative species of the bloom, with no detectable cryptophytes and hardly any other organisms present in the bloom water (Fig. 1*B*). At 1.03×10^6 cells L^{-1}, *M. rubrum* abundance in the bloom was over 100-fold higher than the annual peak in Long Island Sound (15). Each *Mesodinium* cell harbored 20 to 30 cryptophyte cells (n = 16), which packed the peripheral region of the *M. rubrum* cells (Fig. 1*E*), with complete cell structures, including cell membranes, nuclei, and chloroplasts (Fig. 1*C*). Taking advantage of the large cell size of *Mesodinium* spp. (width, 20 to 23 μm; length, 25 to 26 μm), we picked *M. rubrum* cells from samples under the microscope and obtained a 1,581-bp rRNA gene (rDNA) small subunit (SSU) sequence (GenBank accession no. KX781269) and plastid rDNA SSU sequences (GenBank accession nos. KX816859–KX816862), which phylogenetically verified the bloom organism as *M. rubrum* (Fig. 1*D*) and the endosymbiotic alga as *T. amphioxeia* (15). The endosymbiotic *T. amphioxeia* cells contained high amounts of phycoerythrin, indicating that they were photosynthetically active (15).

To investigate what biochemical activities were taking place in these cells, we extracted RNA from the bloom sample and conducted metatranscriptome sequencing using an Illumina HiSeq 2000, generating 39,488,639 raw reads (BioProject ID code PRJNA340945; Sequence Read Archive accession no. SRR4098290), which produced 297,537 unigenes (Table S1). About 164,199 (55.18%) of these unigenes were functionally annotated and the rest were novel genes, whose functions remain to be characterized. The annotated portion of the metatranscriptome was predominated by cryptophyte genes (cryptophyte subset), mainly matching *Guillardia theta* (16) but also *Rhodomonas* sp. (accounting for 58.11% of

Significance

Symbioses between marine plankton species are diverse and widespread both spatially and taxonomically. However, the nature and function of such relationships in natural assemblages are severely underexplored due to technical challenges. Consequently, as an example, the relationship between the ciliate *Mesodinium rubrum* and its observed cryptophyte endosymbiont is varied and debated, from enslaving chloroplasts to exploiting an organelle complex. Applying environmental transcriptomics and other methods to a natural bloom of *M. rubrum* revealed an unsuspected relationship, "host farming symbiont," in which the host helps to transport nutrients from the environment, promotes symbiont cell proliferation, and benefits from the symbiont's photosynthesis.

Author contributions: D.Q. and S.L. designed research; D.Q. performed research; D.Q., L.H., and S.L. contributed new reagents/analytic tools; D.Q. analyzed data; and D.Q. and S.L. wrote the paper.

The authors declare no conflict of interest.

This article is a PNAS Direct Submission.

Freely available online through the PNAS open access option.

Data deposition: The data reported in this paper have been deposited in the National Center for Biotechnology Information (NCBI) BioProject database (ID code PRJNA340945) and Sequence Read Archive (accession no. SRR4098290).

[1]To whom correspondence should be addressed. Email: senjie.lin@uconn.edu.

This article contains supporting information online at www.pnas.org/lookup/suppl/doi:10.1073/pnas.1612483113/-/DCSupplemental.

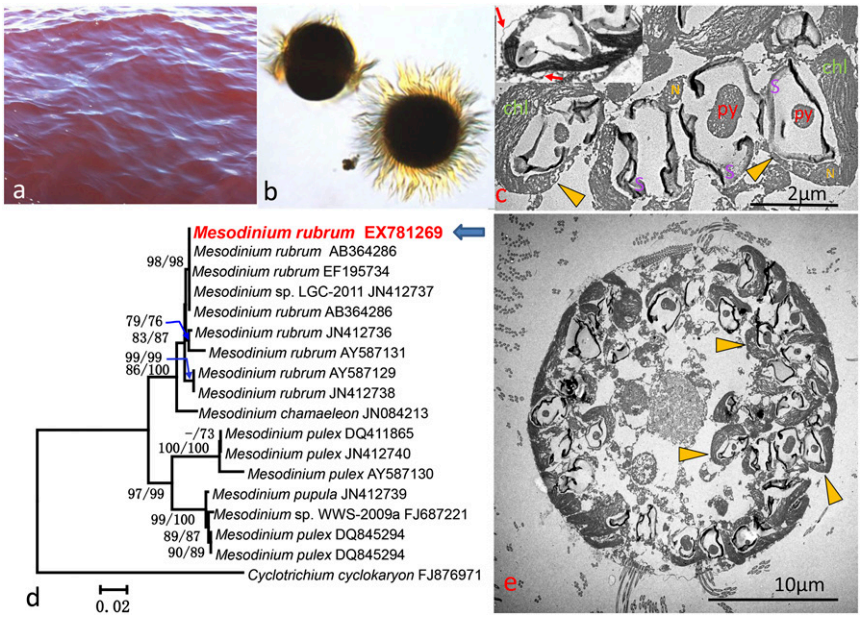

Fig. 1. Red-tide bloom and the causative organisms. (*A*) Photograph of the red tide, which was detected on September 24, 2012, near the University of Connecticut's oceanographic monitoring station (40° 57.01′ N, 73° 35.73′ W), when the water temperature was 21.9 °C and salinity was 27.9. (*B*) Light microscopic image of the causative ciliate, morphologically resembling *M. rubrum*. (*C*) TEM image showing *T. amphioxeia* cells within *M. rubrum*. chl, chloroplast; N, nuclei; py, pyrenoid; S, starch. Yellow arrowheads, *T. amphioxeia* cells; red arrows, cell membrane. (*D*) 18S rDNA phylogenetic tree verifying that the causative ciliate was *M. rubrum*. Values at the nodes are bootstrap values from maximum-likelihood/neighbor-joining analyses. (Scale bar, substitution rate per nucleotide site.) (*E*) TEM image of *M. rubrum* showing many *T. amphioxeia* cells packing the peripheral region of the *M. rubrum* cell.

annotated reads and 11.36% of annotated unigenes), followed by the phaeophyte *Ectocarpus siliculosus*, the pelagophyte *Aureococcus anophagefferens*, and the ciliate *Oxytricha trifallax* (Fig. S1). Less than 1% of the unigenes (2,665) were annotated as ciliate genes, which are enriched in vital processes such as signal transduction, transport and catabolism, cell growth and death, and metabolism of carbohydrate, energy, and amino acids.

The cryptophyte subset of the metatranscriptome contained all major metabolic and regulatory pathways and plasma membrane transporters expected of an intact alga. For photosynthesis, we retrieved light-harvesting components, ATP synthases, electron transport components, and Calvin cycle and C4 pathways (Figs. S2 and S3 and Datasets S1 and S2), and compared them with those in the diatom *Thalassiosira pseudonana* (17). In particular, the phycoerythrin gene was expressed at an extremely high level (Table 1), consistent with the very strong orange fluorescence of phycoerythrin inside *M. rubrum* cells (15). Also highly expressed were chlorophyll a/b-binding proteins (Dataset S1), indicating that *T. amphioxeia* was actively absorbing light energy for photosynthesis and fighting for photoprotection (18, 19).

The metatranscriptome allowed us to provide detailed documentation of core metabolic pathways in a cryptophyte, including the tricarboxylic acid (TCA) cycle, pyruvate metabolism, glyoxylate metabolism, glycolysis/gluconeogenesis, pentose phosphate pathway, propanoate metabolism, fructose metabolism, and starch metabolism (Fig. 2, Fig. S4, and Dataset S3). The crucial connections from the TCA cycle to starch (amylose) and PRPP in the pentose phosphate pathway, and from carbohydrates, amino acids, and lipids to the TCA cycle, were uninterrupted (Fig. 2). Most of the linking enzymes were highly expressed in the bloom. In starch metabolism, we found evidence for synthesis of amylose in the chloroplasts from UDP-glucose and ADP-glucose, with abundant transcripts of granule-bound starch synthase and starch synthase 1. Additionally, we detected a cryptophyte starch-binding domain protein gene, consistent with a large starch structure noted in the periplastid of the endosymbiotic *T. amphioxeia* (Fig. 1*C*). Furthermore, we retrieved alpha-amylase, beta-amylase, and 4-alpha-glucanotransferase transcripts, evidence of alpha-D-glucose production from starch (Dataset S3). For nucleotide metabolism, almost complete cryptophyte biosynthetic and catabolic pathways of purine and pyrimidine nucleotides were identified, comparable to pathways in *Thalassiosira pseudonana* (Fig. 2, Figs. S5 and S6, and Dataset S4) (17).

Proteins and enzymes required for key regulatory pathways, including those in DNA replication and repair, gene transcription, translation, folding, sorting, and degradation, were highly enriched in our cryptophyte submetatranscriptome (Datasets S5–S9). Nuclear gene transcripts responsible for DNA replication, mismatch repair, base excision repair, nucleotide excision repair, spliceosomes, ribosomal proteins, aminoacyl tRNA synthetases, RNA transport, and signal recognition were detected (Fig. S7 and Datasets S5–S7). Importantly, we retrieved transcripts of proliferating cell nuclear antigen, DNA polymerases, and other enzymes related to DNA replication, and also detected cyclin, cyclin-dependent kinase 2, and other genes related to eukaryotic cell growth and division (Table 1 and Datasets S5 and S6). This shows that the endosymbiotic *T. amphioxeia* cells were likely to be proliferating. Meanwhile, transcription and translation genes in the nucleolus, nucleus, nuclear pore, cytoplasm, and chloroplast/mitochondrion were also identified (Table 1 and Datasets S7 and S8).

Furthermore, the majority of the proteins involved in protein processing in the endoplasmic reticulum were found (Fig. S8 and Dataset S9), including genes encoding protein modification and transport as well as endoplasmic reticulum-associated degradation and the ubiquitin pathway. We also found mRNAs encoding ubiquitin-mediated proteolysis and proteasome and RNA degradation (Dataset S9).

The intactness of the plasma membrane and expression of its transporters are key to distinguishing the case of retaining chloroplasts or the organelle complex from that of adopting whole cells as symbionts. We not only observed the membrane around the endosymbiotic cells but also found cDNAs of plasma membrane transporters homologous to those in *G. theta*,

Table 1. Key genes and their expression levels, indicated by RPKM, as evidence that *T. amphioxeia* within *M. rubrum* were intact and functionally active and exported photosynthate to *M. rubrum*

Key enzyme/protein genes	Function	Subcellular localization	RPKM
Photosynthesis			
Phycocyanin	Photosynthesis	Chloroplast	377
Phycoerythrin	Photosynthesis	Chloroplast	39,153
Ribulose-bisphosphate carboxylase large chain	Carbon fixation	Chloroplast	12
Cell-membrane transporters for N-nutrient import and photosynthate export			
AmtB, NH_3 channel protein, formerly NrgA	Ammonium transporter	Cell membrane	142
High-affinity electrogenic NH_3/methylammonia transporter	Ammonium transporter	Cell membrane	321
Likely peptide exporter, ABC superfamily	Peptide exporter	Cell membrane	25
Exocyst complex component 7	Exocyst exporter	Cell membrane	11
Cell division			
DNA polymerase alpha subunit A	Eukaryote DNA replication	Nucleus	17
DNA primase	Chloroplast DNA replication	Chloroplast	3
Proliferating cell nuclear antigen	DNA replication and cell division	Nucleus	90
Cyclin A	Eukaryote cell growth and division	Nucleus	21
Cyclin B	Eukaryote cell growth and division	Nucleus	25
Cyclin-dependent kinase 2	Eukaryote cell growth and division	Nucleus	34
Gene transcription and translation			
DNA-directed RNA polymerases I, II, and III subunit RPABC5	Eukaryote RNA polymerase	Nucleus	34
DNA-directed RNA polymerase subunit beta′	Chloroplast RNA polymerase	Chloroplast	5
GTP-binding nuclear protein Ran	RNA transport	Nucleus	135
mRNA export factor	RNA transport	Nuclear pore	37
Snurportin-1	RNA transport	Cytoplasm	48
Glutamyl-tRNA synthetase	Chloroplast aminoacyl-tRNA biosynthesis	Mitochondrion/chloroplast	119
Glutaminyl-tRNA synthetase	Eukaryote aminoacyl-tRNA biosynthesis	Eukaryote cytoplasm	50
20S proteasome subunit beta 1	Proteasome biosynthesis	Proteasome	170
Large subunit ribosomal protein L4	Chloroplast ribosome biosynthesis	Mitochondrion/chloroplast	24
Large subunit ribosomal protein L4e	Eukaryote ribosome biosynthesis	Cytoplasm	276

indicating that these were genes expressed in the *M. rubrum*-harbored *T. amphioxeia*. These included transporters for inorganic nutrients (nitrate, ammonium, phosphate, and sulfate), organic nutrients (urea), amino acids, and metal ions (Mg^{2+}, Zn^{2+}, Mn^{2+}, and Ca^{2+}) (Table 1 and Dataset S10). Compared with the nitrate transporter [reads per kb of exon per million mapped reads (RPKM) 26; all being high-affinity types], ammonium transporters (RPKM 463) were expressed much more abundantly, including AmtB and a high-affinity electrogenic NH_3/methylammonia transporter (Table 1). Meanwhile, we found very abundant transcripts of ammonium transporters (RPKM 695) and a high-affinity nitrate transporter (RPKM 38) that matched counterparts in alveolate species (*O. trifallax*, *Perkinsus marinus*, and *Vitrella brassicaformis*), indicating that the ciliate host was actively expressing these N-nutrient transporters. These results suggest that ammonium was the major form of N nutrient for the *Mesodinium*–*Teleaulax* system, and came directly (supplied by) or indirectly (acquired from the external environment) through the host. Because the bloom sample was nearly a *T. amphioxeia*-monospecific culture entirely "caged" in the cytoplasm of *M. rubrum* cells (Fig. 1 *C* and *E*) and showed a >20:1 *T. amphioxeia*-to-*M. rubrum* cell concentration ratio, these results indicate functional cell membranes in both the ciliate and symbiotic cryptophyte and a coordinated function in the endosymbiotic entity for nutrient uptake.

Trafficking between organelles would also indicate an endosymbiont beyond an organelle complex arrayed in the ciliate host. We detected cDNAs encoding transporters in the chloroplast membrane, including glucose-6-phosphate/phosphate and phosphoenolpyruvate/phosphate translocators, which facilitate export of photosynthetically produced carbohydrates from the chloroplast to the cytoplasm in exchange for phosphorus import into the chloroplast. Also retrieved were cDNAs of transporters for phosphate, *S*-adenosylmethionine, and aspartate/glutamate; of ABC transporters; of sodium/potassium/calcium exchangers in mitochondria; of an acetyl-CoA transporter in the endoplasmic reticulum; and of transporters for nucleotide sugars (GDP-fucose and UDP-galactose) in the Golgi apparatus (Dataset S10).

Furthermore, we looked for evidence that the symbiont benefited the host. mRNAs were found that encode likely peptide exporter and exocyst complex components (Table 1), which can transport the peptide or other materials from *T. amphioxeia* to *M. rubrum* (Fig. 3). Endomembrane-based protein import and export have been reported in *Geminigera cryophila* as an endosymbiont within *M. rubrum* (20). These findings offer evidence that *M. rubrum* receive photosynthetic products from symbiotic *T. amphioxeia* or *G. cryophila* cells.

All our data in concert demonstrate that the *T. amphioxeia* plasma membrane, plastid, nucleus, mitochondrion, Golgi apparatus, endoplasmic reticulum, and proteasome were retained intact and metabolically active within *M. rubrum* during the bloom (Fig. 3 and Table 1). These endosymbiotic *T. amphioxeia* cells were expressing genes that regulate photosynthesis (including photoprotection), cytoplasmic metabolic pathways, and cell division. More importantly, the two parties of the symbiotic entity seemed to cooperate in nutrient uptake and enabled translocation of photosynthetic products to the host. The necessary regulation and orchestration of all these algal cellular functions would be too extensive for the host ciliate to execute as implied in the model in which only organelles are retained. Rather, our data indicate that the *M. rubrum* population kept intact the *T. amphioxeia* cells they ingested, and were promoting their ability to photosynthesize and reproduce and in return benefited from the photosynthetic products

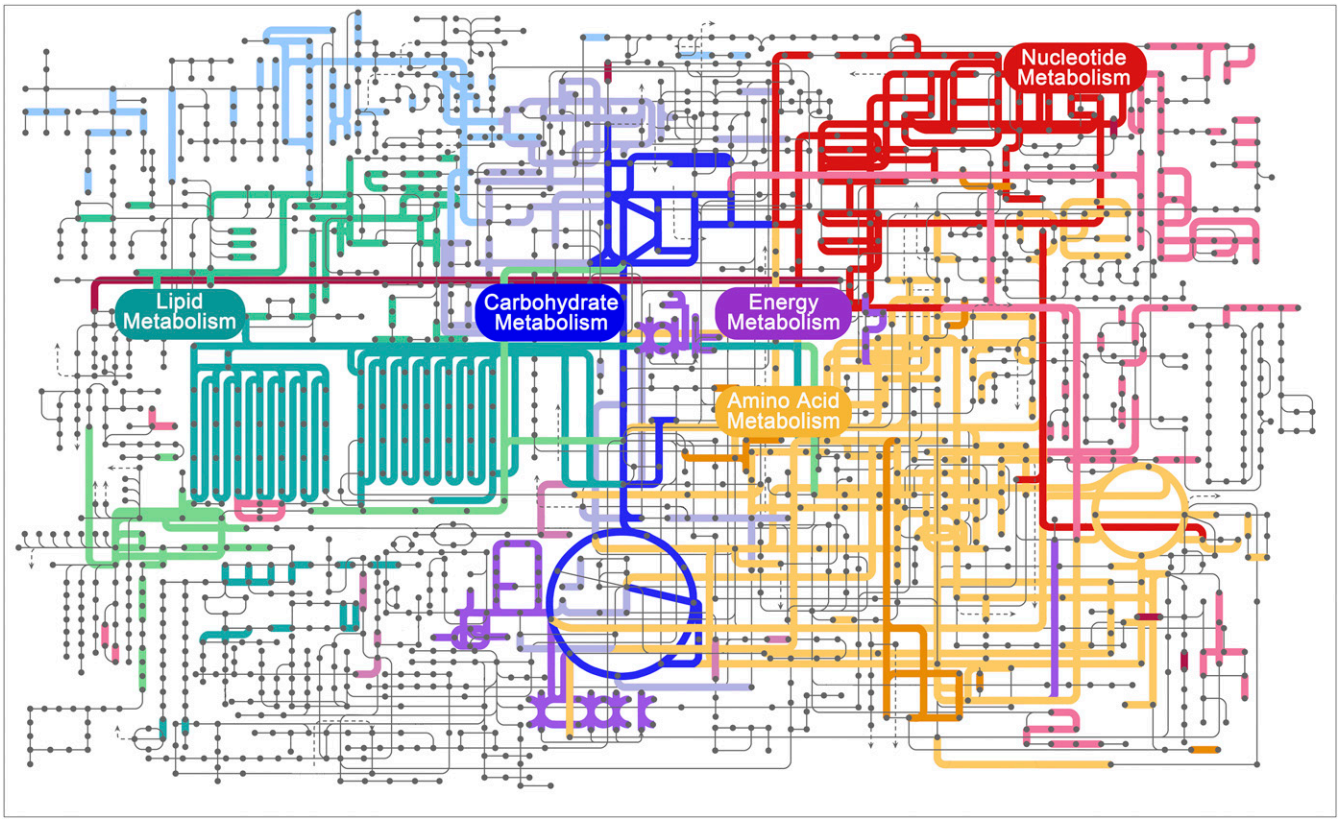

Fig. 2. Metabolic circuit map constructed from the cryptophyte subset of the metatranscriptome. Highlighted in this circuit are pathways of nucleotide metabolism (red), carbohydrate metabolism (blue), energy metabolism (purple), lipid metabolism (cyan), and amino acid metabolism (yellow) in cryptophytes.

(Fig. 3). Consistent with the possibility that the cryptophyte endosymbiont reproduced while in the host, we found that the bloom was equivalent to a bloom of *T. amphioxeia* at a concentration of 2 to 3 × 10^7 cells L^{-1}, almost 100 times higher than the highest *Teleaulax* spp. concentrations we have ever seen in our past 5 y monitoring data in Long Island Sound (~4 × 10^5 cells L^{-1}; Dataset S11). However, this cryptophyte was undetectable in ambient water (Fig. 1). Therefore, *M. rubrum* behaved like a farmer of the cryptophyte.

The *Mesodinium*-farming-*Teleaulax* model not only distinguishes itself from the current model of *Mesodinium* enslaving cryptophyte chloroplasts or the organelle complex, but by promoting the proliferation of the endosymbiotic cells also differs from the conventional whole-cell endosymbiont models in which only binary division synchronous with host division is expected. The disparity from previous studies on *Mesodinium*–cryptophyte symbiosis mentioned earlier might have arisen from the pairing of different *M. rubrum* strains [at least five clades have been identified (21)] with different species or strains of the cryptophyte. The difference can be a result of spatially separated host–symbiont coevolution, as predicted by the geographic mosaic of coevolution theory (22). This and the ecological significance in each case should be further studied in the future.

Materials and Methods

Sampling. Ten liters of surface water was collected in Long Island Sound on September 24, 2012 during a red-tide event, which covered about 20 km^2, an estimation based on remote sensing data (15). The sample was transported to the laboratory and kept in a wide-open bucket to allow ample air exchange overnight; two samples (each 50 mL) were collected by centrifugation for 10 min at 5,000 × *g* (4 °C). The cell pellets were suspended in TRIzol solution and stored at –80 °C until RNA extraction. Another sample was preserved with neutral Lugol's solution and stored in the dark at 4 °C for microscopic analysis.

Analysis for Identities of the Causative Species and Its Plastids. Live and fixed samples were observed under an Olympus BX51 epifluorescence microscope. Microscopic observation of the species was done following Garcia-Cuetos et al. (21). *M. rubrum* cells were isolated with Pasteur pipets, and rinsed carefully with glass fiber membrane (0.7-μm pore size) filtered seawater for subsequent DNA extraction. Twenty of these cells of *M. rubrum* were resuspended in 0.5 mL DNA lysis buffer and incubated for 48 h at 55 °C. DNA extraction, PCR amplification [using a pair of rDNA SSU primers (23, 24) and a pair of plastid rDNA SSU primers (25) (Table S2)], cloning, and gene sequencing for rDNA SSU gene and plastid rDNA SSU gene were conducted with methods outlined previously (25). Sequence alignment and phylogenetic analyses were conducted as previously reported (15).

Observation of Cell Structures of *M. rubrum* and Its Symbionts. Fifty milliliters of bloom sample fixed in 5% (vol/vol) Lugol's was centrifuged at 5,000 × *g* for 10 min and resuspended in 2 mL of 5% (wt/vol) buffered glutaraldehyde fixative and fixed at 4 °C for 48 h. The refixed cells were recentrifuged at 5,000 × *g* for 10 min and resuspended in 0.5 mL of 2% (wt/vol) osmium tetraoxide solution prepared in cacodylate buffer as a poststain and fixative at 4 °C for 12 h. The sediment of osmium-fixed cells was washed in PBS buffer, dehydrated in a graded ethanol/aqueous series and acetone, and embedded in Spurr's resin (SPI-Chem). Ultrathin sectioning, poststaining, and transmission electron microscope (TEM) observation (JEM-100CX II; JEOL) were done as described previously (26).

RNA Isolation and Transcriptome Sequencing. Total RNA was extracted from the collected cells using a TRIzol Reagent Kit (ThermoFisher Scientific) essentially as reported (27), treated with RNase-free DNase I (TaKaRa) to eliminate residual genomic DNA if any, and concentrated and repurified using the RNeasy MinElute Kit (Qiagen). Then, the extracted RNA was determined using the Qubit RNA Assay Kit by a Qubit 2.0 fluorometer (Life Technologies) and NanoPhotometer spectrophotometer (IMPLEN). RNA integrity was verified (6.4 on a scale of 1 to 10) using the RNA Nano 6000 Assay Kit of the Agilent Bioanalyzer 2100 system (Agilent Technologies).

A total of 10 μg RNA was used as input material for Illumina high-throughput sequencing (RNA-seq). The sequencing library was prepared using the NEBNext Ultra Directional RNA Library Prep Kit for Illumina (NEB) following the

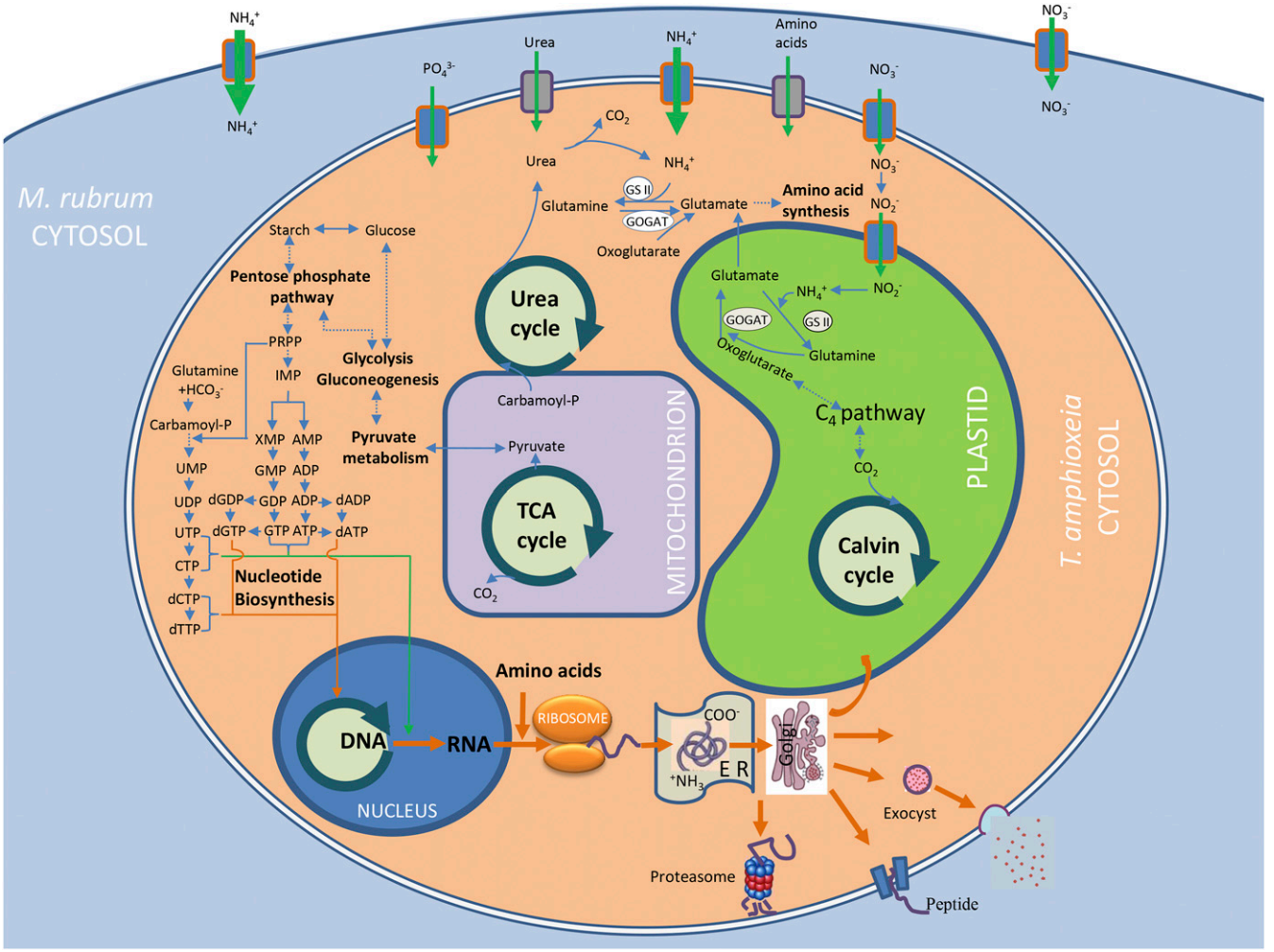

Fig. 3. Schematic summary of key components of nutrient transport and metabolism in *T. amphioxeia* inside *M. rubrum* as well as photosynthate export from the cryptophyte endosymbiont to the ciliate host. Solid arrows indicate direct steps in a pathway, dashed arrows indicate omission of multiple steps in a pathway, and thick arrows indicate genetic information processing and cargo transport.

manufacturer's recommendations (28). Library quality was assessed on the Agilent Bioanalyzer 2100 system. The library preparation was then sequenced on an Illumina HiSeq 2000 platform and paired-end reads were generated.

Bioinformatic Analysis. Transcriptome assembly was accomplished using Trinity (29). The resultant nonredundant unigenes were used for BLAST search and annotation against the NCBI nr database and Swiss-Prot database with a 1e-5 value cutoff, euKaryotic Ortholog Groups (KOG) database with a 1e-3 value cutoff, and Protein family (Pfam) Kyoto Encyclopedia of Genes and Genomes (KEGG) database (30–32). Functional annotation by Gene Ontology (GO) terms was analyzed using the Blast2GO program (33). Genes associated with the major pathways and functions elaborated in this paper were manually reanalyzed using BLAST to verify the functional prediction. The metabolic circuit (Fig. 2) was manually checked to ensure the completeness of the pathways and the connectivity of the major nodes. Furthermore, the expression level of each gene was quantified as reads per kb of exon per million mapped reads to the transcriptome (34). Based on the KEGG Orthology (KO), KOG, and other databases, metabolic network pathways in *T. amphioxeia* were further analyzed using iPath2.0 (pathways.embl.de/iPath2.cgi) (35).

ACKNOWLEDGMENTS. We thank Kay Howard-Strobel, Huan Zhang, and Brittany Sprecher from the University of Connecticut for taking bloom photos and collecting samples, *Teleaulax* spp. cell-count data and advice on sample preparation, and help with English, respectively. Yu Zhong from the South China Sea Institute of Oceanology, Chinese Academy of Sciences helped with TEM sample preparation. We are indebted to Diane K. Stoecker from the University of Maryland and George McManus from the University of Connecticut for insightful discussions. Novogene Bioinformatics Technology Co. Ltd. provided transcriptome sequencing services. The project was supported by the International Collaborative Program of the Natural Science Foundation of China (Grant 41129001 to S.L.), National Science Foundation of the United States (Grant OCE-1212392 to S.L.), Science Technology Program Guangzhou of China (Grant 201607010289 to D.Q.), and Natural Science Foundation of China (Grant 41130855 to L.H.).

1. de Vargas C, et al.; Tara Oceans Coordinators (2015) Ocean plankton. Eukaryotic plankton diversity in the sunlit ocean. *Science* 348(6237):1261605.
2. Johnson MD (2011) Acquired phototrophy in ciliates: A review of cellular interactions and structural adaptations. *J Eukaryot Microbiol* 58(3):185–195.
3. Taylor FJR, Blackbourn DJ, Blackbourn J (1971) The red-water ciliate *Mesodinium rubrum* and its "incomplete symbionts": A review including new ultrastructural observations. *J Fish Res Board Can* 28(3):391–407.
4. Gustafson DE, Jr, Stoecker DK, Johnson MD, Van Heukelem WF, Sneider K (2000) Cryptophyte algae are robbed of their organelles by the marine ciliate *Mesodinium rubrum*. *Nature* 405(6790):1049–1052.
5. Crawford DW (1989) *Mesodinium rubrum*: The phytoplankter that wasn't. *Mar Ecol Prog Ser* 58:161–174.
6. Stoecker DK, Putt M, Davis LH, Michaels AE (1991) Photosynthesis in *Mesodinium rubrum*: Species-specific measurements and comparison to community rates. *Mar Ecol Prog Ser* 73:245–252.
7. Lindholm T (1985) *Mesodinium rubrum*—A unique photosynthetic ciliate. *Adv Aquat Microbiol* 3:1–48.
8. Hibberd DJ (1977) Observations on the ultrastructure of the cryptomonad endosymbiont of the red-water ciliate *Mesodinium rubrum*. *J Mar Biol Assoc U.K.* 57:45–61.

9. Oakley BR, Taylor FJR (1978) Evidence for a new type of endosymbiotic organization in a population of the ciliate *Mesodinium rubrum* from British Columbia. *Biosystems* 10(4):361–369.
10. Johnson MD, Tengs T, Oldach D, Stoecker DK (2006) Sequestration, performance, and functional control of cryptophyte plastids in *Myrionecta rubra*. *J Phycol* 42(6):1235–1246.
11. Johnson MD, Oldach D, Delwiche CF, Stoecker DK (2007) Retention of transcriptionally active cryptophyte nuclei by the ciliate *Myrionecta rubra*. *Nature* 445(7126):426–428.
12. Taylor FJR, Blackbourn DJ, Blackbourn J (1969) Ultrastructure of the chloroplasts and associated structures within the marine ciliate *Mesodinium rubrum* (Lohmann). *Nature* 224:819–821.
13. Lindholm T, Lindroos P, Mörk AC (1988) Ultrastructure of the photosynthetic ciliate *Mesodinium rubrum*. *Biosystems* 21(2):141–149.
14. Hansen JP, Fenchel T (2006) The bloom-forming ciliate *Mesodinium rubrum* harbours a single permanent endosymbiont. *Mar Biol Res* 2(3):169–177.
15. Dierssen H, et al. (2015) Space station image captures a red tide ciliate bloom at high spectral and spatial resolution. *Proc Natl Acad Sci USA* 112(48):14783–14787.
16. Curtis BA, et al. (2012) Algal genomes reveal evolutionary mosaicism and the fate of nucleomorphs. *Nature* 492(7427):59–65.
17. Armbrust EV, et al. (2004) The genome of the diatom *Thalassiosira pseudonana*: Ecology, evolution, and metabolism. *Science* 306(5693):79–86.
18. Peterson RB, Schultes NP (2014) Light-harvesting complex B7 shifts the irradiance response of photosynthetic light-harvesting regulation in leaves of *Arabidopsis thaliana*. *J Plant Physiol* 171(3–4):311–318.
19. Wang H, et al. (2014) The global phosphoproteome of *Chlamydomonas reinhardtii* reveals complex organellar phosphorylation in the flagella and thylakoid membrane. *Mol Cell Proteomics* 13(9):2337–2353.
20. Lasek-Nesselquist E, Wisecaver JH, Hackett JD, Johnson MD (2015) Insights into transcriptional changes that accompany organelle sequestration from the stolen nucleus of *Mesodinium rubrum*. *BMC Genomics* 16:805.
21. Garcia-Cuetos L, Moestrup Ø, Hansen PJ (2012) Studies on the genus *Mesodinium* II. Ultrastructural and molecular investigations of five marine species help clarifying the taxonomy. *J Eukaryot Microbiol* 59(4):374–400.
22. Thompson JN (1994) *The Coevolutionary Process* (Univ of Chicago Press, Chicago).
23. McManus GB, Xu D, Costas BA, Katz LA (2010) Genetic identities of cryptic species in the *Strombidium stylifer/apolatum/oculatum* cluster, including a description of *Strombidium rassoulzadegani* n. sp. *J Eukaryot Microbiol* 57(4):369–378.
24. Zhang H, Lin S (2002) Detection and quantification of *Pfiesteria piscicida* by using the mitochondrial cytochrome *b* gene. *Appl Environ Microbiol* 68(2):989–994.
25. Qiu D, Huang L, Liu S, Lin S (2011) Nuclear, mitochondrial and plastid gene phylogenies of *Dinophysis miles* (Dinophyceae): Evidence of variable types of chloroplasts. *PLoS One* 6(12):e29398.
26. Qiu D, Huang L, Liu S, Zhang H, Lin S (2013) Apical groove type and molecular phylogeny suggests reclassification of *Cochlodinium geminatum* as *Polykrikos geminatum*. *PLoS One* 8(8):e71346.
27. Lin S, Zhang H, Zhuang Y, Tran B, Gill J (2010) Spliced leader-based metatranscriptomic analyses lead to recognition of hidden genomic features in dinoflagellates. *Proc Natl Acad Sci USA* 107(46):20033–20038.
28. Hansen KD, Brenner SE, Dudoit S (2010) Biases in Illumina transcriptome sequencing caused by random hexamer priming. *Nucleic Acids Res* 38(12):e131.
29. Grabherr MG, et al. (2011) Full-length transcriptome assembly from RNA-seq data without a reference genome. *Nat Biotechnol* 29(7):644–652.
30. Altschul SF, et al. (1997) Gapped BLAST and PSI-BLAST: A new generation of protein database search programs. *Nucleic Acids Res* 25(17):3389–3402.
31. Kanehisa M, et al. (2008) KEGG for linking genomes to life and the environment. *Nucleic Acids Res* 36(Database issue):D480–D484.
32. Finn RD, et al. (2008) The Pfam protein families database. *Nucleic Acids Res* 36(Database issue):D281–D288.
33. Götz S, et al. (2008) High-throughput functional annotation and data mining with the Blast2GO suite. *Nucleic Acids Res* 36(10):3420–3435.
34. Mortazavi A, Williams BA, McCue K, Schaeffer L, Wold B (2008) Mapping and quantifying mammalian transcriptomes by RNA-seq. *Nat Methods* 5(7):621–628.
35. Yamada T, Letunic I, Okuda S, Kanehisa M, Bork P (2011) iPath2.0: Interactive pathway explorer. *Nucleic Acids Res* 39(Suppl 2):W412–W415.